Symmetric Diblock Copolymer Thin Films on Rough Substrates. Kinetics and Structure Formation in Pure Block Copolymer Thin Films

E. Sivaniah, Y. Hayashi, S. Matsubara, S. Kiyono, and T. Hashimoto*

Department of Polymer Chemistry, Graduate School of Engineering, Kyoto University, Katsura, Kyoto 615-8510, Japan

K. Fukunaga

UBE Industries, Ltd., 8-1 Goi-minamikaigan, Ichihara, Chiba 290-0045, Japan

E. J. Kramer and T. Mates

Materials Department, University of California at Santa Barbara, Santa Barbara, California 95801

Received September 1, 2004; Revised Manuscript Received November 3, 2004

ABSTRACT: The effect of substrate roughness on the orientation of lamellar microdomains of symmetric poly(styrene)-*block*-poly(methyl methacrylate) [PS-*b*-PMMA] was investigated. Thin films of three molecular weights of PS-*b*-PMMA were prepared on organic polyimide and inorganic indium tin oxide substrates whose surfaces were characterized for roughness and surface energy. It was shown, through cross-section transmission electron microscopy (TEM) and dynamic secondary ion mass spectroscopy (dSIMS), that above a critical substrate roughness all three molecular weights of PS-*b*-PMMA produced a perpendicular lamellar orientation. Using atomic force microscopy (AFM) and PS-*b*-PMMA thin films on an array of polyimide substrates of varied substrate roughness, a critical substrate roughness was identified, below which a parallel orientation was observed. This behavior was modeled simply and showed that the critical roughness determined by AFM represents an underestimate of the true critical roughness of the substrate. Finally, a series of TEM cross sections of thin films on rough and smooth substrates, annealed to different stages of reaching equilibrium, are shown and discussed in terms of the dynamics of ordering in block copolymer thin films.

1. Introduction

Diblock copolymers in general are known for their ability to self-organize into ordered domains and assume a spectrum of different microphase-separated structures, e.g., spherical, cylindrical, gyroidal, or lamellar, that depends principally on the relative amounts of each (immiscible) copolymer block component that is present. This particular property, within a block copolymer thin film configuration, is currently being harnessed to produce nanoscopic structures that can be put to various uses, e.g., templates for synthesis of organic/inorganic hybrids, mesoporous membranes, or nanopatterning of substrates.[1]

The lamellar microdomain structure in unconfined block copolymer thin films, bounded by flat nonneutral substrate and air interfaces, assumes a so-called parallel orientation; i.e., the interfaces of the microphase-separated blocks are arranged parallel to the substrate plane. This orientation arises because the bounding surfaces induce an attractive field for one component of the block copolymer that promotes the growth of composition fluctuations normal to the surface. As first predicted by Fredrickson,[2] surface-directed ordering of block copolymer has been observed in lieu of the randomly oriented ordering process, originating from the interior of the thin film and at temperatures at which the block copolymer, in its bulk state, would normally be disordered.[3,4] Thus, a slowly decaying, oscillatory chemical potential field (with a periodicity roughly proportional to that of the copolymer radius of gyration) emanates from the air and substrate surfaces into the thin film. For very thin films, fields originating from the surface and substrate interact at temperatures below the bulk order−disorder transition. For the case where these interactions are out of phase, lateral mass transport in the plane of the thin film is induced so that the film surface roughens, thickening and thinning in various places, leading ultimately to the formation of island−hole structures at the free surface.[5,6] Fasolka and Mayes give a comprehensive review of the notable advances in the understanding of block copolymer thin film behavior.[7]

More recent research has focused on frustrating surface directed parallel orientation in order to produce a perpendicular orientation of the lamellae with respect to the substrate plane. Logically, these efforts have sought to alter the surface generated field. Hence, the substrate surface chemistry was adjusted to create a "neutral" surface,[8] or the substrate was patterned with a laterally repeating chemical pattern that alternately attracted each component of the block copolymer.[9,10] In the former case, the absence of a surface-directing field produces a perpendicular lamellar orientation in thin films for entropic reasons; i.e., a perpendicular orientation in a thin film geometry provides more ways to arrange the microdomain interfaces than the parallel orientation. In the latter case the growth of lateral composition fluctuations is encouraged over those normal to the substrate, provided there is coherence between the periodicities of the lamellar domains and the lateral pattern. Perpendicular orientations are also induced by confinement of block copolymer films. This occurs when the confined films are of a thickness that

* Corresponding author. E-mail Hashimoto@alloy.polym.kyoto-u.ac.jp.

10.1021/ma0482157 CCC: $30.25
Published on Web 02/02/2005

normally produce island−hole structures in its unconfined state.[11] Alternatively, imposing an external field that is stronger than the existing surface directed fields is another route to creating perpendicular orientations, e.g., temperature gradient,[12] electric,[13−15] and solvent fields.[16,17]

The effect of a roughened substrate topography on block copolymer microdomain orientation in thin films has received scant attention given the natural abundance of rough substrates. An archetypal rough surface has a roughness of q_sR, where $q_s \equiv 2\pi/\lambda_s$. R is the (root-mean-square) vertical displacement of the surface topography about a mean horizontal plane. λ_s is the characteristic lateral periodicity in the surface topography. Ideal, grating-like substrates (of $q_sR \sim 0.15$) have been studied with lamellar block copolymer thin films, giving rise to the alignment of island−hole defects with the substrate periodicity.[18] Larger aspect ratio grating substrates have been used in nonlamellar systems, but the mechanisms for ordering in these cases are the coordinated surface directed ordering from the base and the side walls of the grating substrate.[19,20]

In a recent communication we noted that e-beam deposited indium tin oxide (ITO) coatings on glass have similar though less ideal substrate topologies with a well-defined q_sR.[21] The lateral periodicity and structure arise from crystallization of the ITO alloy during deposition. We observed the lamellar orientation in thin films of a single molecular weight of poly(styrene)-*block*-poly(methyl methacrylate) [PS-*b*-PMMA] on these substrates. Our results showed that a rough ITO substrate (with high q_sR) produced perpendicular lamellae throughout the thin film. Polyimide (PIM) replicas of the rough ITO produced identical orientations. Annealing the PIM replica surface above its glass transition produced a smooth (low q_sR) substrate. Parallel oriented PS-*b*-PMMA was observed on this substrate. We thus showed that substrate roughness rather than substrate neutrality was responsible for the appearance of perpendicular lamellae in our work.

This current paper expands on these previous results. In section 3.1, we demonstrate through cross-sectional transmission electron microscopy (TEM) that the observation of perpendicular lamellar orientation on rough substrates is general to a range of PS-*b*-PMMA molecular weights. We also obtain a quantitative analysis of the depth profiles of parallel and perpendicular lamellae using dynamic secondary ion mass spectroscopy (dSIMS). In sections 3.2 and 3.3, respectively, we discuss experimentally and via modeling the transition from a perpendicular to parallel orientation on rough substrates. Finally, in section 3.4 we discuss the effects of substrate roughness on the kinetic development of orientation in the thin film. An in-depth analysis of the lamellar periodicity of the perpendicular structures as a function of molecular weight is left to a future paper.[22]

2. Experimental Details

2.1. Substrate Preparation and Characterization. A variety of substrates are discussed in our study. Our original substrates are e-beam deposited ITO and sputter coated ITO substrates, purchased from Furuchi Chemical Co. (Tokyo, Japan). Generally, sputter coating is performed at lower vacuum pressure than e-beam deposition and leads to markedly smoother ITO surfaces. Henceforth, these sputter-coated substrates are referred to as smooth ITO (S_ITO). Two batches of the rougher e-beam coated ITO substrates were used in this study. The two batches had roughness values, q_sR, that differed by a factor of 2 and are referred to as supercritically rough ITO (SC_ITO) and undercritically rough ITO (UC_ITO) for reasons that become apparent in section 3.4. It is also possible to prepare polyimide (PIM) substrates whose surfaces replicate the topographical features of the ITO surface. A solution of polyamic acid composed of biphenyltetracarboxylic acid and oxydianiline was spun-cast onto SC_ITO substrates. Curing at 300 °C for 2 h in air produced 100 nm thick films of the corresponding polyimide with an expected glass transition temperature of 260−270 °C. This supported film was submerged in a hydrochloric acid bath that etched away the underlying ITO substrate and released the PIM layer. The PIM film, floating on the surface of the HCl bath, was then picked up onto an glass support substrate in such a way so as to have the replicated rough polyimide (SC_PIM) surface topmost. A smooth PIM substrate (S_PIM) was also prepared by spin-casting and annealing the polyimide precursor onto a glass substrate. All substrates were ultrasonically cleaned in mild organics prior to use.

The roughness of these substrates was characterized using atomic force microscopy (AFM; Nanoscope III Multimode, from Digital Instruments, Santa Barbara, CA). A typical surface topography and surface height profile of SC_ITO, UC_ITO, and S_ITO substrates are shown in Figure 1 and its insets. From such AFM images we can extract the rms roughness (about a mean horizontal plane), R, using AFM software. Similarly, the characteristic lateral length scale associated with this roughness was extracted using a 2-dimensionally averaged power spectral density analysis (PSD) of the AFM images (Figure 2). From this figure it is noted that both types of rough ITO have a maximum in the power spectral density at lateral length scales, λ_s, of ∼150 nm (corresponding to $q_s = 0.04$ nm^{-1}) with a variation of ∼±50 nm full width at half-maximum (fwhm). The intensity of the spectra for the two types of rough ITO reflects the differences in the vertical roughness parameter R. SC_ITO and UC_ITO had R values of 14.5 ± 1.5 and 8 ± 1 nm, respectively. Smooth ITO has larger characteristic lateral length scale, λ_s, of ∼400 nm ($q_s = 0.016$ nm^{-1}) and values of R of 3.2 ± 0.5 nm.

It is important to comment about the variation in the roughness of our rough ITO substrates. The ITO coatings are commercially prepared in large batches, so that deposition conditions and hence surface roughness, q_sR, can differ from batch to batch by as much as 50%. Even within a particular batch of ITO glass, q_sR can vary from one 10 × 10 cm^2 (as received) substrate to the other by 10%. These substrates are then cut to 1 cm^2 pieces for our analysis. Within this area, q_sR does not vary by more than 5%.

Figure 2 also shows that a PIM replica of supercritically rough ITO, designated as unannealed SC_PIM, has almost the same spectral features as the original, indicating the efficiency of the replication method. Such PIM substrates were ultrasonically cleaned with chloroform before being annealed at temperatures between 265 and 290 °C for a range of times. This resulted in the decrease in the characteristic height (R) of the polyimide substrates. The power spectra of AFM images of such PIM replica substrates after annealing show that there is a slight drift to a larger λ_s for the smoothest of these substrates. By preparing several such samples, we assembled an array of substrates of the same chemical composition but with different roughness. Prior to their use, an easily identifiable area (∼100 × 100 mm^2) on each substrate was designated, and the variation in roughness within this region was characterized. These substrates, where q_sR varied from 0.14 ± 0.016 to 0.48 ± 0.020 in approximate increments of 0.05 or less, are discussed in section 3.2. The roughness values of these substrates can be found from the vertical axis of Figure 8.

At a further point in this paper it is necessary to estimate the difference of the interfacial tensions of PS and PMMA with our various substrate surfaces at an annealing temperature of 200 °C. This difference, $\gamma_{subs,PS} - \gamma_{subs,PMMA}$, is generically referred to as δ_{subs}. Therefore, the contact angles of low molecular weight anionically synthesized PS (M_w = 2K) and PMMA (M_w = 1K) on ITO (rough and smooth) and polyimide

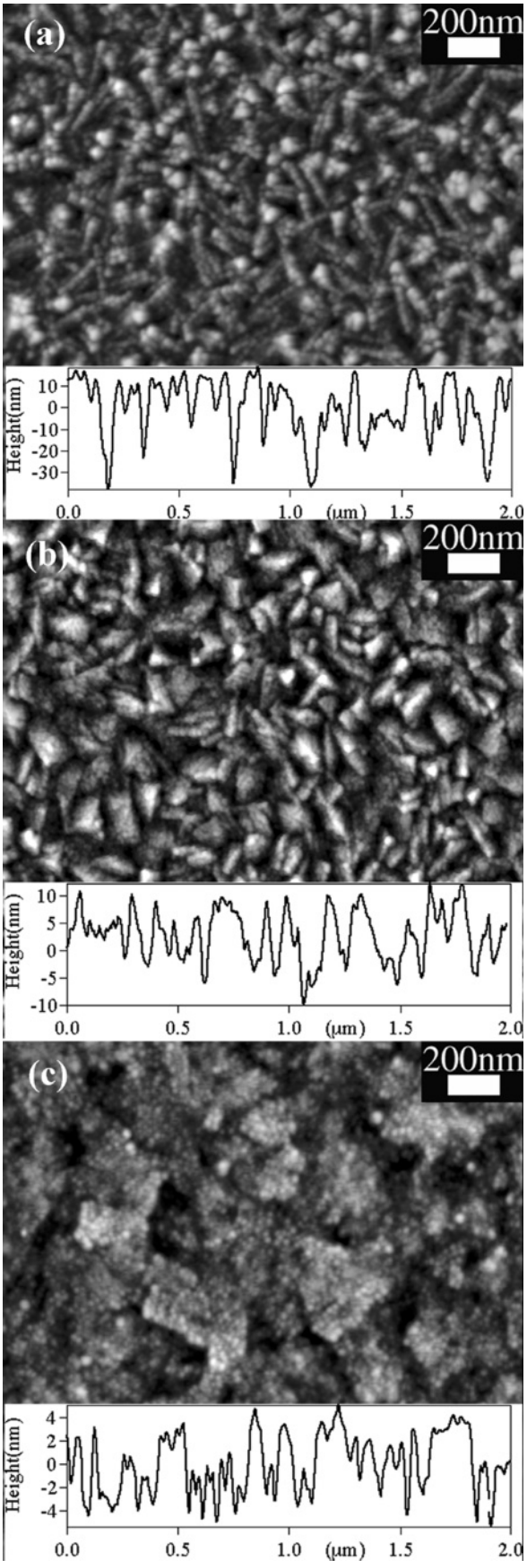

Figure 1. Height mode AFM images of three types of ITO substrate surfaces used in this study: (a) SC_ITO, (b) UC_ITO, and (c) S_ITO. Typical height profiles across the sample surface are given beneath each figure.

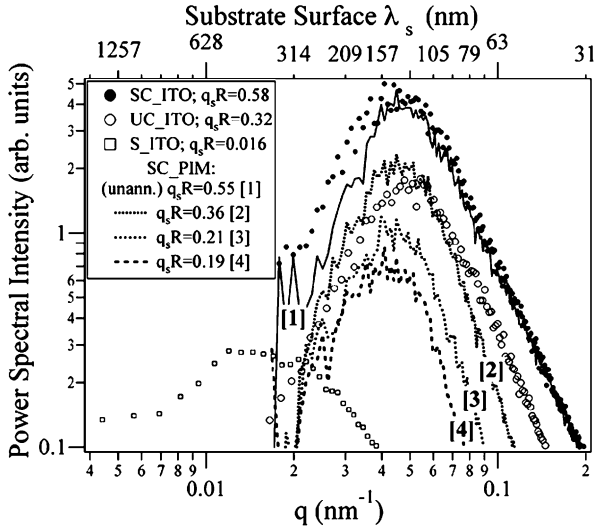

Figure 2. Power spectral analysis of AFM images from a number of substrates used in this study. The symbols refer to spectra of SC_ITO (●), UC_ITO rough (○), and S_ITO (□). The lines correspond to a supercritically rough PIM substrate (line 1) that have been annealed to different degrees of smoothness (lines 2−4).

(smooth) substrates were measured using AFM via a method described by Vitt and Shull.[23] Ultrathin (approximately 10 nm) films of each polymer were spun-cast onto the surfaces of the substrates, annealed at 200 °C for 1−2 h, quickly quenched to room temperature, and then analyzed with AFM. The contact angle θ was calculated from the expression $\tan(\theta/2) = h/r$, where h and r are the height and radius of a dewet polymer droplet. Surface roughness can induce some of the dewet droplets to have noncircular contact lines. Neglecting such droplets, values of h and r were collected for droplet radii ranging from 1 to 3 μm. The θ values of both PS and PMMA on smooth ITO were found to be respectively $\theta_{S\_ITO,PS}$ as 10.4 ± 2.3° and $\theta_{S\_ITO,PMMA}$ as 5.9 ± 1°; on undercritically rough ITO these were found to be respectively $\theta_{UC\_ITO,PS}$ as 10.2 ± 4.5° and $\theta_{UC\_ITO,PMMA}$ as 7.9 ± 3.5°. The larger deviations in the latter set of contact angles are probably associated with substrate roughness effects. We take contact angle $\theta_{ITO,PS}$ and $\theta_{ITO,PMMA}$ to be the average of these two sets of data. δ_{ITO} can be expressed through Young's equation as $\gamma_{air,PMMA} \cos \theta_{ITO,PMMA} - \gamma_{air,PS} \cos \theta_{ITO,PS}$. The literature quoted values for $\gamma_{air,PMMA}$ and $\gamma_{air,PS}$ at 200 °C are 27.8 and 27.4 mN/m.[24] Since, despite these measurements, we later assume that at 200 °C the surface tensions of PS and PMMA are equivalent; we use a value of 27.6 mN/m for $\gamma_{air,PMMA}$ and $\gamma_{air,PS}$. Then δ_{ITO} is found to be 0.25 mN/m.

Because of large variances in the measured contact angles of PS and PMMA on smooth PIM, it was not possible to use the above method to determine the difference in substrate interfacial tensions. We employed group contribution methods in order to estimate δ_{PIM}. The dispersive and polar components of the surface tension of the respective polymers that make up the interface were determined by the van Krevelene group contribution method;[25] the interfacial tension is then calculated via the harmonic mean equation. Using literature reported group parameters,[24,26] we found δ_{PIM} to vary as a function of temperature according to Table 1. This table shows, in accordance with the later dSIMS results, that PMMA has a greater affinity for the PIM substrate and also, as expected, that δ_{PIM} is a decreasing function of temperature and is similar, at 200 °C, to δ_{ITO}.

2.2. Materials and Experimental Analysis. We obtained anionically synthesized symmetric PS-*b*-PMMA diblocks (Polymer Source Inc., Canada) of different molecular weights with low polydispersities (M_w/M_n < 1.06). In this paper, three molecular weights were studied and are referred to as PS-*b*-PMMA(18K−18K), PS-*b*-PMMA(38K−36.8K), and PS-*b*-PMMA-

Table 1. Interfacial Tensions of PS and PMMA and Their Difference, δ_{PIM}, with a PIM Substrate As Determined from Group Contribution Methods

temp (°C)	$\gamma_{PIM,PS}$ (mN/m)	$\gamma_{PIM,PMMA}$ (mN/m)	δ_{PIM} (mN/m)
50	4.442	4.146	0.296
100	4.176	3.916	0.260
150	3.947	3.701	0.246
200	3.734	3.501	0.233
250	3.534	3.315	0.219

(50K−54K), where the numbers in parentheses are the molecular weights of the respective polymer blocks in units of a thousand. An additional block copolymer dPS-*b*-PMMA-(37K−43K) containing a deuterated PS block was also used for dSIMS experiments.

Block copolymer thin films of various thicknesses (ranging from 100 nm to 1.6 μm) were spun-cast from toluene solutions onto the substrates discussed above and dried overnight (at 60 °C) before annealing in a nitrogen-purged oven. The samples were observed after annealing at a range of temperatures (between 200 and 230 °C) and times (from a few minutes up to 2 days). Specific annealing conditions will be given in the subsequent text. A previous report on bulk order−disorder transitions indicates that all our polymers should microphase separate at these annealing temperatures.[27]

The sample structure was observed with tapping mode AFM, TEM, and dSIMS. For TEM observation, the PS-*b*-PMMA film was released from the ITO substrate (by etching out via immersion in HCl) and picked up on a pre-cross-linked epoxy surface. The epoxy assembly was then cut in ultrathin (∼50 nm) cross sections using a Reichert-Nissei Ultracut-S cryo-ultramicrotome using methodologies described previously.[28] A JEOL (JEM2000FXZ) (JEOL, Tokyo, Japan) transmission electron microscope operated at 120 kV was used for observation of the cross sections. For better TEM contrast, these sections were stained by exposure to RuO_4 vapor so that the styrene block of the PS-*b*-PMMA appears darker in our figures.

dSIMS analysis was carried out on a pure dPS-*b*-PMMA film annealed on various substrates. The instrument (Physical Electronics 6650 dynamic SIMS) produces a 3 keV, 60−70 nA beam of O^{2+} ions at 60° off normal incidence, which rasters over a 100 × 100 mm^2 region. Simultaneously, the rastered area was flooded with a static, defocused, 0.7−1 keV electron beam to prevent surface charging effects. Negative ions of 2H-(D), C, and Si were monitored as a function of time from an electrically gated area that was 10% of the rastered area. An experimental Gaussian variance is expected under such conditions with a half-width at half-maximum, σ_e, of 5−7.5 nm, depending on the instrumental parameters. The technique is discussed in detail by other works.[29,30]

The raw output from a dSIMS measurement is the count intensity of a particular set of negative ions vs etch time. These data must be converted into a volume fraction (or concentration) vs depth profile. Coulon et al. reported that the etch rate of PS and PMMA thin films by an O^{2+} ion beam differed by a factor of 1.5. They also reported that the overall etch rate of a blended PS/PMMA thin film was identical to that of a PS film when PS forms the majority component of the blend. Following Coulon et al., we analyze dSIMS data only from the dPS component but apply a simpler etch time/thickness calibration. All our samples have a nondeuterated PS cover layer (of ellipsometrically measured thickness) that isolates the transient effects of the beam damage during the initial establishment of a steady-state damage condition. Therefore, there is a lag time, t_{lag}, before the dSIMS mass spectrometer detects a significant D^- ion signal. This delay time is assumed proportional to the cover layer thickness, and the constant of proportionality is used to scale the depth axis.

The effect of a difference in etch rate between the dPS and PMMA portion will be most apparent when the block copolymer is in its parallel orientation. Generally we expect to see peaks of the deuterated signal separated by areas where the PMMA layers are. If the dPS and PMMA blocks were of similar lengths, we would expect to see the widths of the dPS layers being larger than their separation, largely due to the differential etch effects. In our system, 37K−46K dPS−PMMA, we actually find the dSIMS peak-to-peak distance of the PS layers and their separation are similar (see Figure 4a). This follows since the PMMA layer thickness that should in reality be larger has been etched at a faster rate. Although we have tried to take this into account by scaling the PS and PMMA domain thicknesses with f_{dPS} and $(1 - f_{dPS})$, respectively, the difference in PS and PMMA domain sizes, ∼4 nm, is below the resolution of dSIMS; i.e., this level of detail in the fit is probably unnecessary. Another regime where the difference in etch rate would be a factor is when the orientation is 100% perpendicular. In this case, the initially flat films will begin to roughen as the perpendicular PMMA domains are etched faster than the perpendicular PS domains. Because the incident O^{2+} ions impinge on the film at an angle, the PMMA domains will only differentially etch to a certain depth beyond which any further etching is limited by the shadow effect of the taller, more slowly etching PS structures. This differential-etch-induced roughness will be transmitted through the film during the dSIMS analysis. However, it would be difficult to notice this effect without stopping the dSIMS while the ion beam was midway through the etching of the dPS−PMMA layer. After the beam has reached the underlying PIM layer, the etch-induced roughness would disappear if the PIM is more etch resistant than either PS or PMMA.

The D^- ion count intensity is converted to volume fraction as follows: The "effective" film thickness, l, of the dPS−PMMA film is assumed to be the distance between the two half-heights of the initial rising and final falling edges of the D^- ion signal. A normalization factor can then be determined by equating the integral of the D^- ion data over this thickness range to the average volume fraction of the dPS in the block copolymer. This factor

$$\frac{f_{dps} l}{\int_0^l I^{D^-}(z)\, dz} \tag{1}$$

is applied to the raw counts data. Here f_{dPS} is $N_{dPS}/(N_{dPS} + N_{PMMA})$ and $N_{dPS(PMMA)}$ is the number of segments in the dPS-(PMMA) block; $I^{D^-}(z)$ is the raw D^- dSIMS data as a function of depth z.

3. Experimental Results

3.1. Structure of PS-*b*-PMMA Block Copolymers on Rough and Smooth Substrates. (a) TEM Observation. A previous communication had shown that a single molecular weight of PS-*b*-PMMA (38K−36.8K) produced perpendicular orientation when annealed on supercritically rough ITO substrates at 230 °C for 5 h. Cross-sectional TEM images of thin PS-*b*-PMMA films in Figure 3 show that this phenomenon is general to range of PS-*b*-PMMA molecular weights. In particular, parts a and d of Figure are thin films of 18K−18K and 50K−54K PS-*b*-PMMA, which have been annealed on SC_ITO at 230 °C for 18 and 25 h, respectively. Parts b and c of Figure 3 respectively show 38K−36.8K PS-*b*-PMMA annealed on SC_ITO at 230 °C for 5 and 18 h, suggesting that by 5 h the sample has already reached an equilibrium perpendicular state that does not alter upon further annealing. The interface between the thin film cross sections and the substitute epoxy substrate is quite smeared in these figures, making it difficult to identify the near-surface morphology. The apparent tilt in many of the lamellae in these micrographs may easily be the result of mechanical deformation during the sectioning process.

(b) dSIMS Analysis. TEM images provide a direct visualization of such block copolymer thin films. From

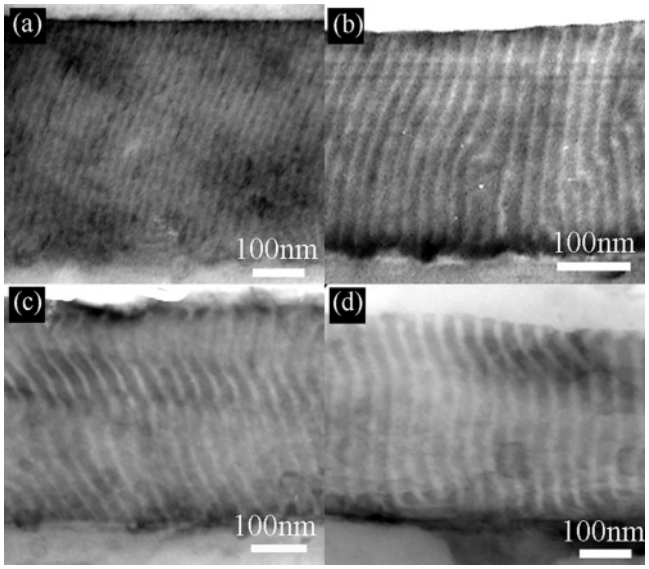

Figure 3. Cross-sectional TEM images of various molecular weight PS-*b*-PMMA thin films annealed at 230 °C on SC_ITO: (a) 18K−18K, (b) 38K−36.8K, (c) 38K−36.8K, and (d) 50K−54K annealed for 18, 5, 18, and 25 h, respectively.

these images of PS-*b*-PMMA annealed on SC_ITO (Figure 3a−d) and SC_PIM substrates[21] the inference is that the entire thin film is in the perpendicular state.

Depth profiling methods such as neutron reflectometry[31] or dSIMS produce large-area-averaged depth profiles of the block copolymer thin film components and provide statistical proof for the TEM derived conclusion. Therefore, dPS-*b*-PMMA(37K−43K), a block copolymer resembling the PS-*b*-PMMA(38K−36.8K) system, was spun-cast onto rough (SC_ITO, SC_PIM) and smooth (S_PIM) substrates. These films were then annealed at 230 °C for 6 h before analysis with dSIMS. In the dSIMS result shown in Figure 4a there are high amplitude oscillations in the dPS volume fraction depth profile, ϕ_{dPS}, for a dPS-*b*-PMMA film annealed on the smooth PIM substrate. These oscillations are due to the predominant formation of parallel lamellae and are nonexistent in the dSIMS analysis of a dPS-*b*-PMMA film annealed on rough ITO (Figure 4b). The lack of oscillations in Figure 4b is prescribed to the predominance of a perpendicular orientation. Oscillations are present but severely damped for dPS-*b*-PMMA films on the rough PIM substrate (Figure 4c), suggesting, in this case, that only a minor fraction of the block copolymer film is in a parallel orientation.

The data in Figure 4a were fit with the following function

$$\phi_{dPS}^{||}(z) = 0.5\left\{\sum_{i=1}^{n}\mathrm{erf}\left[\frac{z - D(i-0.5)p - D(i-1)s}{\sqrt{2}\sigma}\right] - \sum_{i=1}^{n-1}\mathrm{erf}\left[\frac{z - D(i-0.5)p - iDs}{\sqrt{2}\sigma}\right] - \lim_{\sigma\to 0}\mathrm{erf}\left[\frac{z - D(n-0.5)p - D(n-0.5)s}{\sqrt{2}\sigma}\right]\right\} \quad (2)$$

where σ takes the values of σ_{wid} (2 nm from Fernandez et al.[32]) or ~0 depending on whether the interface being

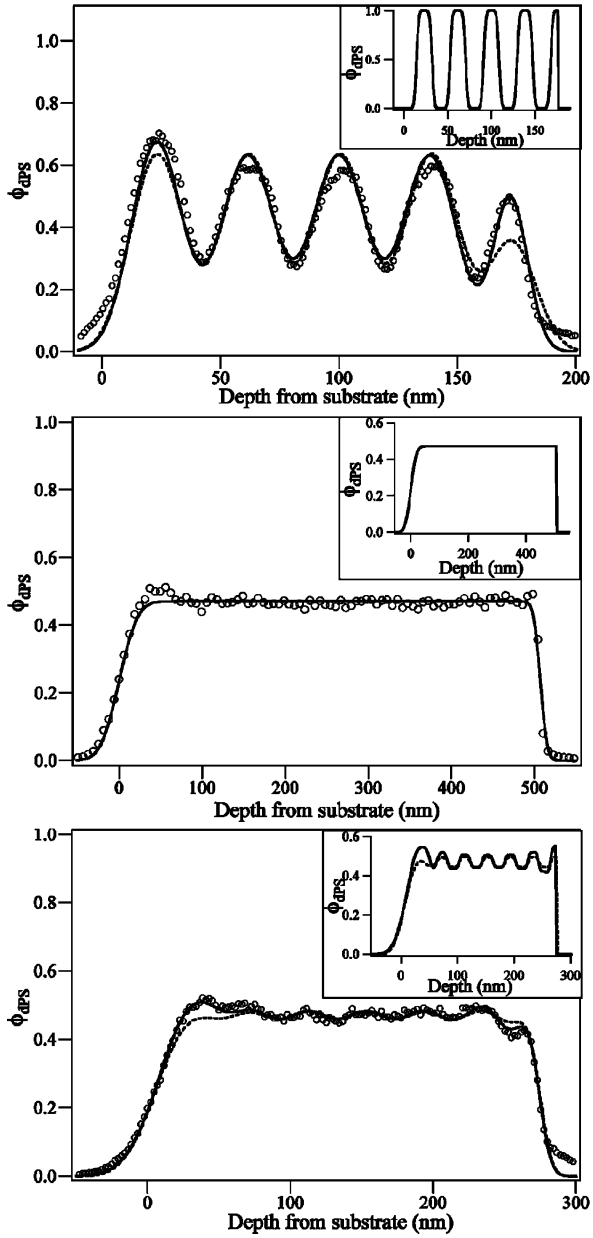

Figure 4. dSIMS data for dPS-*b*-PMMA(37K−46K) thin films annealed on (a) S_PIM, (b) SC_ITO, and (c) SC_PIM. Part a shows fits using a single (see dashed line) or depth dependent (see full line) σ_e parameter. Fits to parts b and c use a depth dependent σ_e. In part c, the dashed line and full lines correspond respectively to a depth independent fit, $f_z^{||} = 0.05$, and a depth dependent fit (see eq A). The insets to the figures give the deconvoluted fit profile.

described is at the block copolymer junction or at the thin film bounding surfaces. Equation 2 essentially describes a periodic series of n dPS layers; closest to the substrate ($z = 0$) is a PMMA substrate surface-wetting layer of thickness $Dp/2$. The subsequent $n - 1$ dPS layers of thickness Ds are alternated with $(n - 1)$ layers of PMMA of thickness Dp. Finally, this series of layers is terminated by a PS air surface-wetting layer of thickness $Ds/2$. s and p are set as f_{dPS} and $1 - f_{dPS}$, respectively; these assumptions are based on higher resolution noninvasive depth profiling analyses of PS-*b*-PMMA parallel lamellae.[33]

The analytic form of eq 2 remains unaltered after its convolution with the Gaussian folding function

$$\frac{1}{(2\pi)^{1/2}\sigma_e} e^{-z^2/2\sigma_e{}^2} \quad (3)$$

which describes the smearing due to instrumental resolution and is characterized by a resolution parameter, σ_e. However the generic interfacial width parameter, σ^2, in eq 2 is now defined as $\sigma_{wid}{}^2 + \sigma_e{}^2$ (or $\sigma_e{}^2$ at the dPS-*b*-PMMA film bounding surfaces).

Thus, n, D, and σ_e are used to fit the data in Figure 4a. In a first fitting attempt (see dashed line in Figure 4a) it was assumed that σ_e did not vary with etch depth. A best fit using a single σ_e value of 9.6 nm—higher than the expected value for this instrument (~5−7 nm)—did not adequately fit the air surface peak (at $z \sim 180$ nm). Since PS-*b*-PMMA is prone to ion beam damage, we proposed that the instrumental resolution is depth dependent; therefore, a bulk resolution parameter, $\sigma_{e,bulk}$, was defined for data collected from the interior of the thin film. This resolution parameter, $\sigma_{e,bulk}$, was distinct from $\sigma_{e,surf}$ and $\sigma_{e,subs}$, the resolution parameters within (arbitrarily) 50 nm of the air and substrate interfaces, respectively. In this way, a superior fit to the data (see full line in Figure 4a) was possible using the more reasonable value of $\sigma_{e,surf}$ as 6.6 nm with the resolution deteriorating within the PS-*b*-PMMA film to a $\sigma_{e,bulk}$ value of 9.9 nm before improving near the substrate; $\sigma_{e,subs} = 8.9$ nm. The ideal (i.e., with no instrumental smearing) profile for this fit is shown as an inset to Figure 4a. From this analysis, D was found to be 38.4 nm—similar to the value extracted from AFM measurements of the perpendicular structures, 40 nm.[34] To maintain consistency, the depth dependent resolution parameters were carried over to fitting of the subsequent data in Figure 4b,c.

Figure 4b, the data of PS-*b*-PMMA on SC_ITO, most easily resembled a system with no parallel orientation and was therefore fit with a single-layer model

$$\phi_{dPS}^{\perp} = 0.5 f_{dps}\left(\mathrm{erf}\left[\frac{z}{\sqrt{2}\sigma_{subs}}\right] - \mathrm{erf}\left[\frac{z-l}{\sqrt{2}\sigma_{surf}}\right]\right) \quad (4)$$

σ_{surf} was set as $\sigma_{e,surf}$, and σ_{subs} was set as $\sqrt{\sigma_{rms}{}^2+\sigma_{e,subs}{}^2}$, since the rough ITO used in this study had a (AFM determined) root-mean-square roughness, σ_{rms}, of ~14 nm. Hence, the only fitting parameter to these data was the thickness of the film. Within the constraints of maintaining $\sigma_{e,surf}$ and $\sigma_{e,subs}$ at a constant value for all three sets of data, a reasonable agreement (see full line Figure 4b) to the data was possible; this suggests that the dPS−PMMA film on the SC_ITO substrate contains virtually no parallel oriented component $\phi_{dPS}^{||}(z)$ and almost completely a perpendicular component $\phi_{dPS}^{\perp}(z)$.

In Figure 4c, a dPS−PMMA thin film has been annealed on a SC_PIM. The oscillations in the dSIMS data suggest that a small area fraction of the film, defined as $f_z^{||}$, can be described by $\phi_{dPS}^{||}(z)$ (cf. eq 2), whereas the remainder is described by eq 4. Therefore, we apply the following general fitting model

$$\phi_{dPS}(z) = f_z^{||}\phi_{dPS}^{||}(z) + (1 - f_z^{||})\phi_{dPS}^{\perp}(z) \quad (5)$$

Clearly, eq 5 is an area averaged description, taking in the simultaneous dSIMS signals of parallel and perpendicular orientations at equal depths, z, but coming from different points within the dSIMS sampled area of the thin film.

Within the parallel oriented component, the intrinsic width of the polymer/polymer interfaces, σ_{wid}, will be broadened near the rough substrate to σ_{wid}' as

$$\sigma_{wid}' = \sqrt{\sigma_{wid}{}^2 + \sigma_{rms}{}^2 e^{-z/z_1*}} \quad (6)$$

where $z = 0$ is identified with the PIM/PS-*b*-PMMA interface. z_1^* describes the characteristic length over which the substrate roughness is transmitted as the roughness of the PS and PMMA interfaces within the lamellar stack and is set, as suggested by Turner and Joanny,[35] as $3/(Dq_s{}^2)$, i.e., 47 nm. Constraining the film thickness of the parallel and perpendicular component expressions in eq 5 to be equivalent, only $f_z^{||}$, D, and n remain as fitting parameters for the data in Figure 4c.

The simplest form of $f_z^{||}$ is to assume it to be a constant, defined as $f_{bulk}^{||}$. The dashed line in Figure 4c represents such a fit, $f_{bulk}^{||}$ (=0.05). n and D were found to be 7 and 41 nm, respectively. The variation in D from the value obtained for Figure 4a is relatively minimal given the inherent errors that can arise in the etch time/depth conversion procedure. This fitting result indicates that the interior of the film is predominantly (95%) perpendicular. The fit was, however, unsatisfactory in the near surface and substrate regimes. A fit that allows for enhanced parallel ordering at the thin film bounding surfaces produced a better account of the near surface dSIMS data (solid line in Figure 4c). Since we cannot draw a full conclusion from this single data set, a description of that more refined fitting procedure is relegated to the Appendix.

In summarizing the dSIMS analysis, we find that a smooth PIM substrate gives rise to parallel oriented lamellae. By using a SC_PIM substrate, 95% of the substrate film appeared to have a nonparallel, and here assumed perpendicular, orientation. By contrast, the rough ITO substrate, SC_ITO, appeared to give 100% perpendicular lamellae. It should be noted that the thickness of the dPS-*b*-PMMA films varied within the sample set discussed here. This may account for the presence of a small component of parallel oriented lamellae in the dSIMS result on the SC_PIM substrate. Generally, however, these results agree with our previous TEM observations.

(c) Film Thickness Effect. Parts a and b of Figure 5 show AFM images of PS-*b*-PMMA(18K−18K) films of 180 and 960 nm thickness, respectively. A similar pair of images is given in parts c and d of Figure 5 for PS-*b*-PMMA(50K−50K) films of 60 and 720 nm thickness, respectively. All samples were annealed on SC_ITO at 230 °C for 5 h. The lamellar spacing, D, can be determined by analyzing the AFM images by fast Fourier transform analysis.[22] There was no effect of film thickness on the lamellar spacing of these films. However, there is plainly an increase in the number of defects (of the type highlighted by an arrow in Figure 5a) for thinner films, indicating that the typical grain size of perpendicular lamellae is smaller in the thinner films.

The number of defects in a given 5 μm square AFM image was counted for a range of film thicknesses for each of the three molecular weights used in this study. From this number, the surface defect concentration per unit area, C_{def}, could be calculated. $C_{def}{}^{-1/2}$ can in turn be considered as a characteristic dimension of the grain

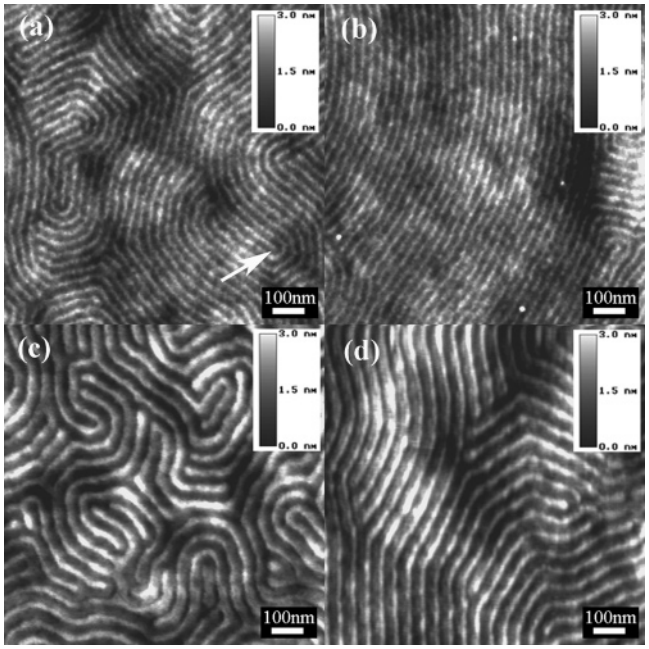

Figure 5. AFM images of PS−PMMA block copolymers of different molecular weight and thickness annealed on SC_ITO at 230 °C for 6 h: (a) 18K−18K, 180 nm; (b) 18K−18K, 960 nm; (c) 50K−54K, 60 nm; (d) 50K−54K, 720 nm.

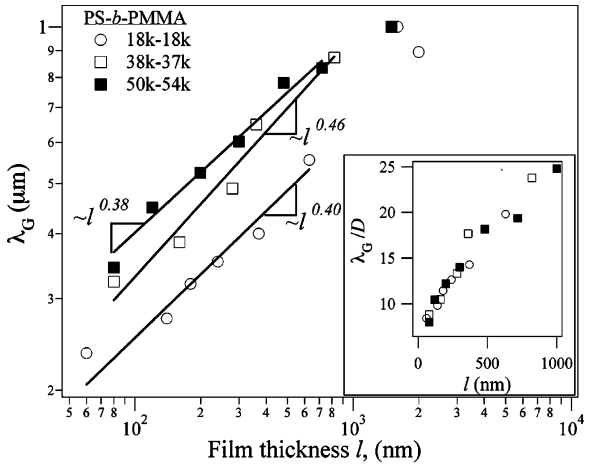

Figure 6. Characteristic microdomain grain size, λ_G, at the surface of 18K−18K, 38K−36.8K, and 50K−54K PS-*b*-PMMA thin films plotted vs film thickness. The inset shows the renormalized data, λ_G/D.

for the perpendicular lamellae at the air surface, λ_G. Thus, the surface defect analysis is plotted as λ_G vs film thickness, l, in Figure 6. Two features of this plot are apparent. First, λ_G for all three molecular weights appears to increase as $l^{0.42}$ with a variation in the exponent of ±0.04 (the individual exponents for each molecular weight are given in Figure 6). Second, the grain size, λ_G, for a particular film thickness appears to increase with molecular weight. It was then found that, by rescaling the grain size with the lamellar spacing as λ_G/D, it was possible to collapse the data for all three molecular weights to a single curve (see inset to Figure 6). Although these are strong results, their meaning is as yet ambiguous.

To some extent, these results on grain size have to take into dynamics of perpendicular grain formation. The initial block copolymer grains will be smaller than the film thickness and will grow three-dimensionally until the grain size is somewhat larger than the film thickness. Once this happens the grain boundaries are dominantly normal to the film. At this stage the substrate roughness will play an important role since the grain boundaries will have a minimum length where the block copolymer film is thinnest, i.e., at positions corresponding to asperities in the underlying substrate. For the boundaries to migrate further laterally the grain boundary area would have to increase and likewise the total energy. The substrate asperities thus play a role similar to the grain boundary grooves that develop in thin crystalline metallic or ceramic films.[42] Because of these effects, the block copolymer grain growth slows and eventually reaches a terminal size. However, the data in Figure 6 refer to the perpendicular lamellar grain size at the air surface. To fully comprehend these results, further work is necessary whereby we can determine the three-dimensional shape of the grains.

3.2. Experimental Determination of Critical Roughness. Previously we have shown that whereas a SC_ITO and SC_PIM (with q_sR of 0.58) produced perpendicular lamellae, a SC_PIM substrate that had been annealed to flatness resulted in parallel orientation of the block copolymer lamella.[21] Thus, logic suggests that there is a critical roughness below which parallel lamellae are observed and above which perpendicular lamellae persist. We determined to find the critical roughness for PIM substrates, since these were ones where it was possible to systematically alter the amplitude of the substrate roughness.

Therefore, 250 nm thin films of PS-*b*-PMMA(38K−36.8K) block copolymer were spun-cast onto an array of polyimide substrates of different roughness; the samples were then annealed at 200 °C for a range of times and their structures observed iteratively with AFM between anneals.

During annealing, three types of block copolymer surface images were successively observed on *most* of the substrates. After the initial anneal, a perpendicular lamellae surface structure (see Figure 7a) was observed for PS-*b*-PMMA films on all of the rough substrates. Aside from the high-frequency height modulations due to the PS-*b*-PMMA perpendicular structures, the thin film surface was relatively smooth. For a substrate with a given q_sR, smaller than a critical value described below, the perpendicular surface structure persisted for a time, t_{q_sR}, after which the thin film surface structure began to show signs of surface roughening (Figure 7b). More protracted annealing of the substrate then led to increased surface roughening, a disappearance of the perpendicular lamellae, and the eventual formation of parallel lamella structures at the air surface as evidenced by lamellar terracing in some portions of the film (see Figure 7c). It was observed that there was a longer lag time, t_{q_sR}, before the thin films on higher q_sR polyimide substrates showed the signs of surface roughening. In the case of very high q_sR substrates this transition did not occur at all, and a perpendicular surface structure was observed at all times (up to 2 days).

Figure 8 summarizes this behavior for the PIM substrates studied and indicates, at a given time, the roughness of the substrates upon which the block copolymer thin film surface structure contained only perpendicular lamellae (filled symbols). The figure also shows the point at which each of these substrates, upon prolonged annealing, began to show signs of forming parallel lamellae (open symbols). The locus of the times

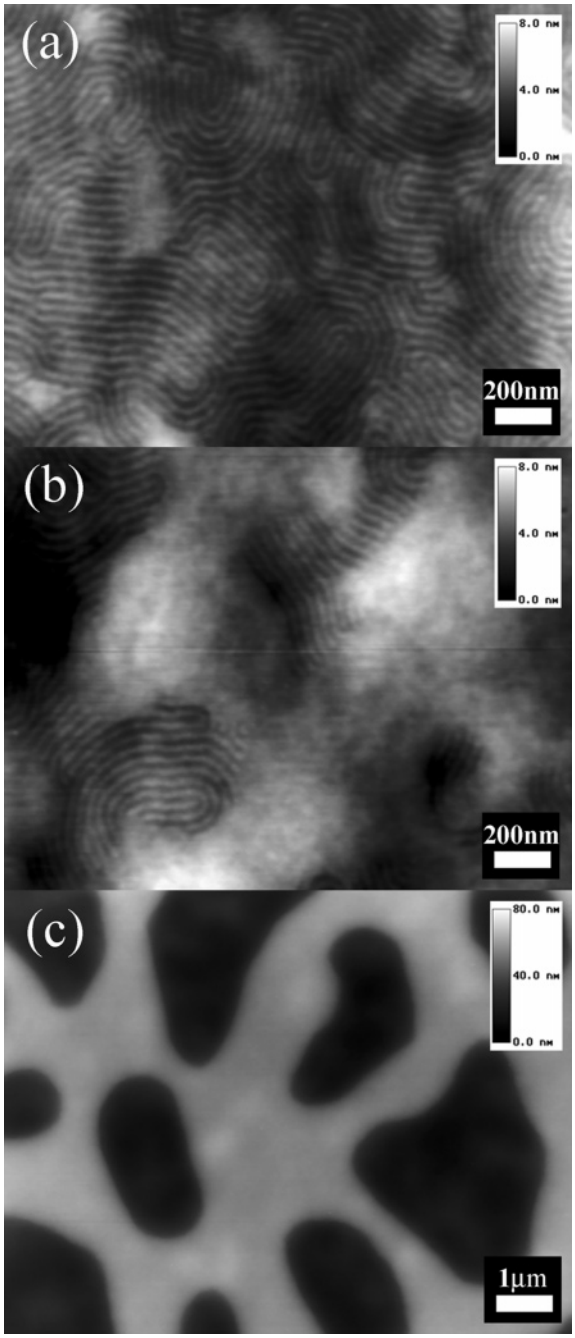

Figure 7. AFM images of 38K−36.8K PS−PMMA block copolymers on a SC_PIM substrate that have been thermally smoothed to a q_sR of 0.25. Images show typical surface states after annealing at 200 °C for increasing times: (a) perpendicular surface state, 60 min; (b) partially perpendicular surface state, 70 min; (c) parallel surface state, 1 day.

where the filled symbols become open ones (as a function of q_sR) is delineated within the figure. At long enough times this locus was found to level off at a roughness of 0.37 ± 0.02; this is identified as the critical roughness, $(q_sR)_{c,AFM}$, of the substrate for 38K−36.8K PS-*b*-PMMA on the polyimide substrate at 200 °C. However, since only samples with a 250 nm PS-*b*-PMMA film thickness were used, it is not known how this critical roughness varies with film thickness.

The PIM substrate samples were rewashed in chloroform to remove the block copolymer; this procedure did not alter the substrate q_sR values. Subsequently, a lower molecular weight block copolymer, 18K−18K PS-*b*-PMMA, of identical thickness (250 nm) was spun-cast onto the PIM substrates, and the entire procedure was repeated. The generic sequence of surface structural changes described previously (and by Figure 7) was also observed for this molecular weight system. The results for this block copolymer are also shown in Figure 8 and suggests a critically rough substrate, $(q_sR)_{c,AFM} \sim 0.41 \pm 0.02$ for 18K−18K PS-*b*-PMMA. Considering the inherent uncertainty in the q_sR of our substrates, it cannot be confidently suggested that the observed trend, of lower $(q_sR)_{c,AFM}$ values for higher molecular weight PS-*b*-PMMA, is appropriate; nonetheless, the repeatability of the overall behavior is reassuring.

We must be careful in interpreting the significance of the AFM-observed critical roughness phenomena and $(q_sR)_{c,AFM}$. To do so, we anticipate portions of the discussion in section 3.4. There we will propose that substrate roughness and surface neutrality can similarly attenuate the extent of surface directed ordering in block copolymer thin films. In the absence of surface directed ordering, perpendicular lamellar orientations are prevalent in thin films. However, if allowed, surface-directed parallel orientation will proliferate at much faster rates than the intrinsic ordering of a perpendicular oriented grain.

In our system we assume the air surface is neutral so that in its vicinity perpendicular lamellae are prevalent, initially as small sized grains that grow with time. As a result, the propensity of these perpendicular grains to be consumed by parallel oriented grains through a process of defect annihilation decreases with time. Simultaneously, substrate surface directed ordering is occurring to an extent that is determined by the substrate roughness. If the substrate directed ordering can occur fast enough (i.e., at low substrate roughness), it will be able to consume the small sized perpendicular lamellar grains formed near the air surface. Then a fully parallel lamellar system will be realized (Figure 9a).

If substrate directed ordering is slower (i.e., for a higher substrate roughness), the near surface perpendicular lamellae can grow too large to be consumed by the approaching parallel lamellar front. An essentially metastable state is reached, which we observed through AFM to be a stable perpendicular lamellar state but which actually has a mixed set of orientations within the film (Figure 9b). Thus, any of the filled symbols with roughness above $(q_sR)_{c,AFM}$ in Figure 8 can represent this state. Hence, $(q_sR)_{c,AFM}$ represents the roughness where parallel lamellae, if formed at the substrate, do not have enough driving force to reach the air surface. At the higher, true critical substrate roughness, $(q_sR)_{c,true}$, the substrate roughness fully attenuates the substrate surface directed formation of parallel lamellae so that only perpendicular lamellae are formed in the thin film (Figure 9c). With AFM alone, we cannot identify which of the PIM substrate roughnesss above $(q_sR)_{c,AFM}$ represents $(q_sR)_{c,true}$. However, from our cross-sectional TEM results of PS-*b*-PMMA on replica polymide substrates we know that $(q_sR)_{c,true}$ should be less than or equal to 0.58 since fully perpendicular lamellae were observed on these substrates.

In this above description the assumption of air surface neutrality, i.e., the equality of PS and PMMA surface tensions has not been verified; however, literature reports[24] suggest that this is the expected trend at high enough temperatures. We continue to invoke this assumption in what follows.

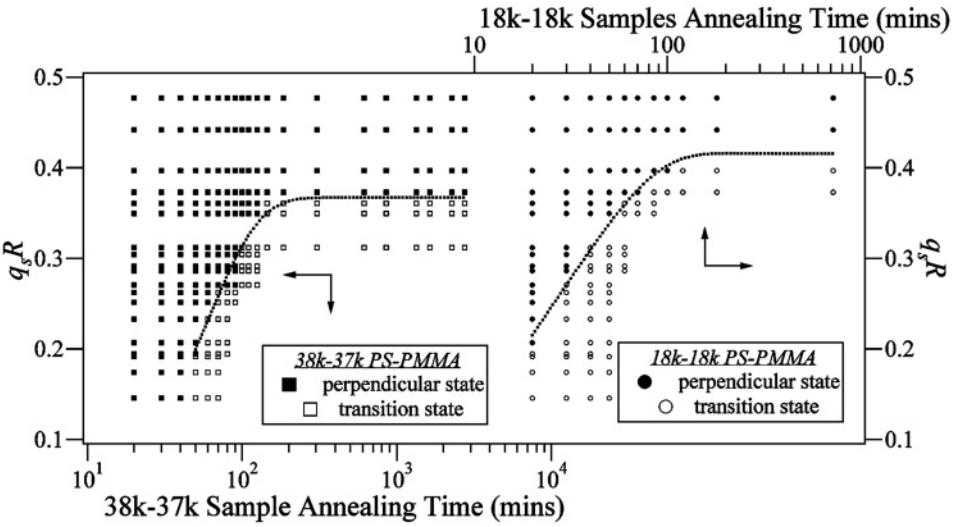

Figure 8. Summary of AFM analysis of 18K−18K (squares) and 38K−36.8K (circles) PS−PMMA films annealed on an array of PIM substrates of a range of q_sR values. The full and open symbols indicate surfaces found to be in a fully perpendicular (cf. Figure 7a) and mixed (cf. Figure 7b) surface state. The dotted lines indicate the locus of t_{qR} from one state to the other.

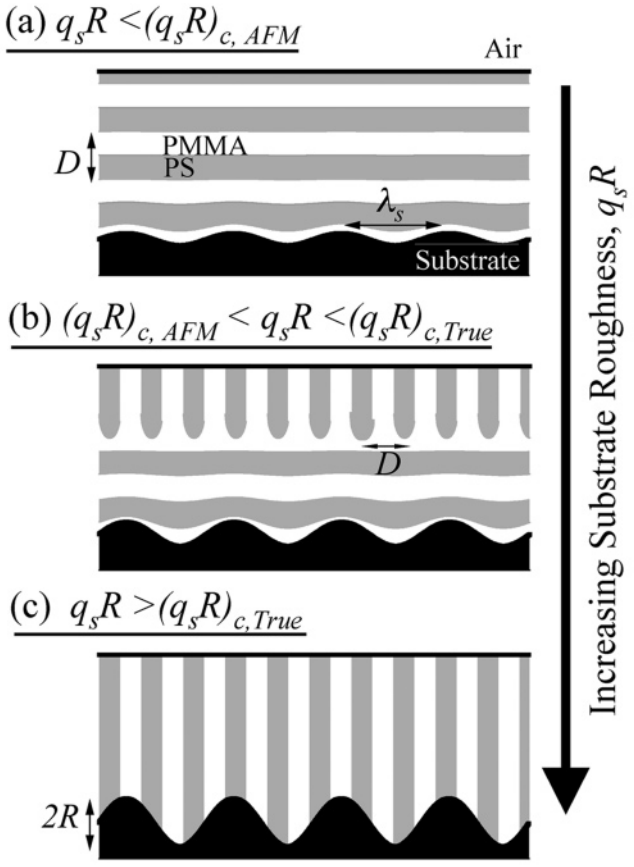

Figure 9. A schematic of the interior of block copolymer thin films (a) below the AFM observed critical substrate roughness, $(q_sR)_{c,AFM}$, (b) above $(q_sR)_{c,AFM}$, and (c) above the true critical substrate roughness, $(q_sR)_{c,true}$. The gray and unshaded areas refer to the PS and PMMA portions of the microdomain structure, respectively. The dark lines and black shaded areas refer to the air and substrate interfaces interfaces, respectively.

3.3. Discussion of Critical Roughness Effect. One way to understand the existence of a critical substrate roughness, $(q_sR)_{c,true}$, that dictates block copolymer orientation is to compare the main free energy penalties, ΔF, for each orientation, perpendicular ($\perp$) and parallel ($\parallel$), due to a rough substrate, relative to a reference state of parallel lamellae on a smooth substrate. The rough substrate will increase the free energy of a parallel oriented thin film through bending deformations of the lamellae. The principal energy penalty for perpendicular lamellae on rough surfaces arises from unfavorable contacts between the block copolymer components and the substrate. For a sufficiently rough substrate such comparison may lead the perpendicular configuration to be more energetically favorable.

We can estimate the relative free energies of these two orientations using a simple model, illustrated in Figure 10. We use a simplified substrate with a single sinusoidal surface topology, having an amplitude R and lateral periodicity λ_s ($\equiv 2\pi/q_s$). Other simplifying assumptions of the model are that the mean film thickness of both the parallel and perpendicular orientations is equal to an integral number of lamellar periods, D, and that D is constant, irrespective of lamellar orientation or position within the film. The film thickness is also considered sufficiently large so as to neglect the surface-normal compressive forces that would be substantial for monolayer thick block copolymers films on the rough substrates. In view of our experimental system we make the assumption that $\lambda_s \gg D > R$. The changes in free energy due to substrate roughness of each system per unit projected area in the substrate plane is calculated assuming a reference state of a parallel oriented lamellar thin film on a smooth substrate (Figure 10a).

In the parallel system (Figure 10b), we assume a "asymmetric" system without losing any generality, i.e., that the PMMA block prefers the substrate interface ($\gamma_{subs,PMMA} < \gamma_{subs,PS}$), and PS is arranged as the air-wetting layer for the parallel geometry. This surface and substrate wetting behavior is also assumed for the reference state. Moreover, the deformations to the parallel lamellae due to the rough substrate are assumed to have decayed by the point the air surface is reached.

The calculation of the free energy, $\Delta F^{\parallel}$, of a parallel stack of lamellar block copolymers on a sinusoidal modulated substrate of roughness q_sR was considered in detail by Turner and Joanny and through scaling arguments by Pickett et al. and most recently by Tsori and Andelman.[36,37] Because of the relative explicitness

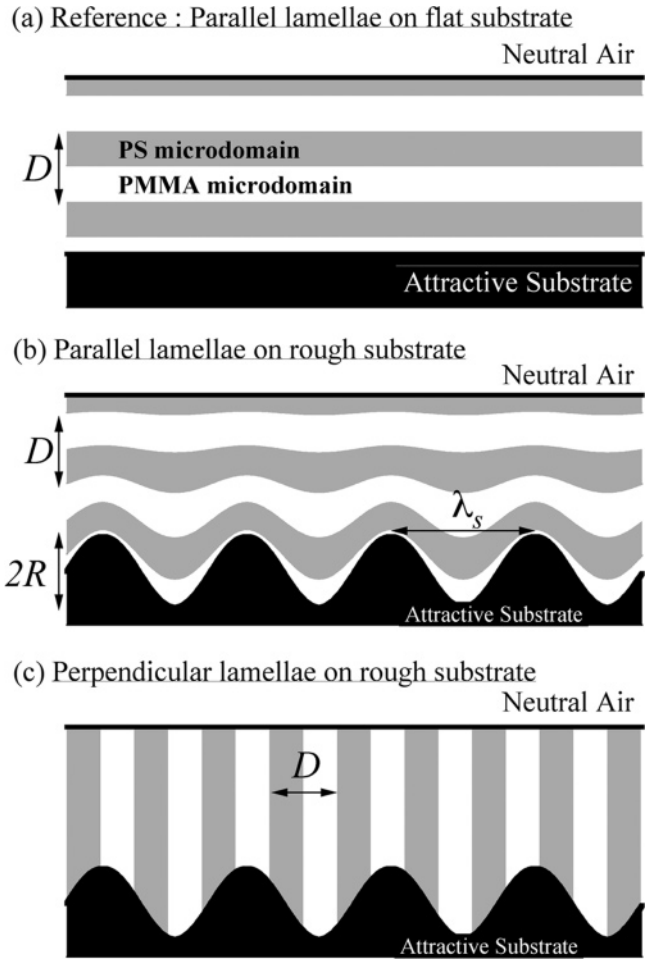

Figure 10. A schematic of the model block copolymer thin film structure used to determine $(q_sR)_{c,true}$: (a) the reference state of a parallel set of lamellae on a smooth attractive substrate with a neutral air surface; (b) the deformation of the parallel lamellae on a rough attractive substrate; (c) the perpendicular orientation on the same rough attractive substrate.

of Turner and Joanny's (TJ) treatment, we use many of their results in this paper. Using the above assumptions, the free energy of a parallel stack of lamellae on a rough substrate can be expressed as

$$\Delta F^{\parallel} = \frac{\beta R^2}{6z_1^*} + \gamma_{\text{subs,PMMA}} \frac{(q_sR)^2}{4} \tag{7}$$

The first term of this expression is the increase in free energy due to deformation of the lamellar block−block interfaces. β is the compression modulus of the block copolymer chain ($\equiv 3\gamma_{\text{PS,PMMA}}/D$) (from TJ), and z_1^*, defined earlier, is the characteristic length over which a sinusoidal deformation arising from the substrate is transmitted into the interior of the lamellar stack. The second term simply expresses the increase in substrate interfacial area as a result of the substrate corrugation.

In determining $\Delta F^{\perp}$, we assumed the perpendicular configuration (Figure 10c) persists throughout the film and neglect the increase in free energy of the perpendicular system due to local chain distortions near the substrate−block copolymer interface. The condition $\lambda_s \gg D$ implies that such distortions are local and not transmitted laterally through the block copolymer. Such an assumption was recently verified by Tsori et al., who found that the decay length of lateral perturbations to a set of perpendicular lamellae is $\sim D$, i.e., a factor of $\sim(\lambda_s/D)^2$ smaller that the decay length for vertical perturbations to a set of parallel lamellae. $\Delta F^{\perp}$ is then simply the difference of the substrate and air interfacial interactions with both components of the block copolymer:

$$2\Delta F^{\perp} = (\gamma_{\text{subs,PMMA}} + \gamma_{\text{subs,PS}})[(q_sR)^2/4] + \delta_{\text{subs}} + \delta_{\text{air}} \tag{8}$$

Equating the two free energies and taking into account air surface neutrality ($\delta_{\text{air}} = 0$), there is a value, $(q_sR)_{c,true}$

$$(q_sR)_{c,true}{}^2 = \frac{3\delta_{\text{subs}}}{\gamma_{\text{PS,PMMA}} - 0.75\delta_{\text{subs}}} \tag{9}$$

that defines a critical roughness above which perpendicular lamellae are more energetically favored. From earlier calculations, $\delta_{\text{PIM}} \sim \delta_{\text{ITO}} \sim 0.25$ mN/m and $\gamma_{\text{PS,PMMA}}$ at 200 °C is taken as 1 mN/m.[38] Thus, we can find a predicted $(q_sR)_{c,true}$ as 0.96. Taking into account that our experimentally determined value of $(q_sR)_{c,AFM}$, ~0.4, should be an underestimate of the $(q_sR)_{c,true}$ and that our rough substrates have only a formal resemblance to the ideal substrates used in the TJ-based prediction, an order of magnitude agreement is very respectable.

There are clear weaknesses to our expression for $(q_sR)_{c,true}$. The TJ analysis, performed via a weak perturbation of a flat substrate topology, is more suitable to cases where $q_sR \ll 1$. Moreover, the analysis is performed within the strong segregation limit, where block junctions are specifically located at the block copolymer domain interfaces; the systems observed in this paper are more weakly segregating. As a result, the model cannot produce the molecular weight dependence to $(q_sR)_{c,true}$ that is alluded to from the experimental data. By contrast, the more sophisticated model of Tsori et al. takes into account the effect of lamellar periodicity; in a future paper we shall present detailed comparisons of our experimental results with their theoretical predictions.

3.4. Dynamics of Structure Formation. It was noted from Figure 8 that even though PS-*b*-PMMA annealed on undercritically rough polyimide substrates eventually resulted in the formation of parallel lamellae, the initial lamella structure observed at the surface of the thin film has a perpendicular orientation. Then, interestingly, the thin film surface structure for films on rougher (though still undercritically rough) substrates take a longer time to produce evidence of parallel orientation. It is difficult to interpret this phenomenon on the basis of AFM studies alone. Therefore, using cross-sectional TEM, we observed the changes in interior structure of ~400 nm thick PS-*b*-PMMA(38K−36.8K) films as a function of annealing time. PIM substrates were not used in these experiments solely because of the difficulty of preparing cross sections from these replica substrates. Instead, UC_ITO and S_ITO were used to mimic the PIM substrates, since these had nominally similar surface energies. UC_ITO has a general q_sR of 0.32 ± 0.04 and is an order of magnitude rougher than S_ITO. Both substrates are less than critically rough.

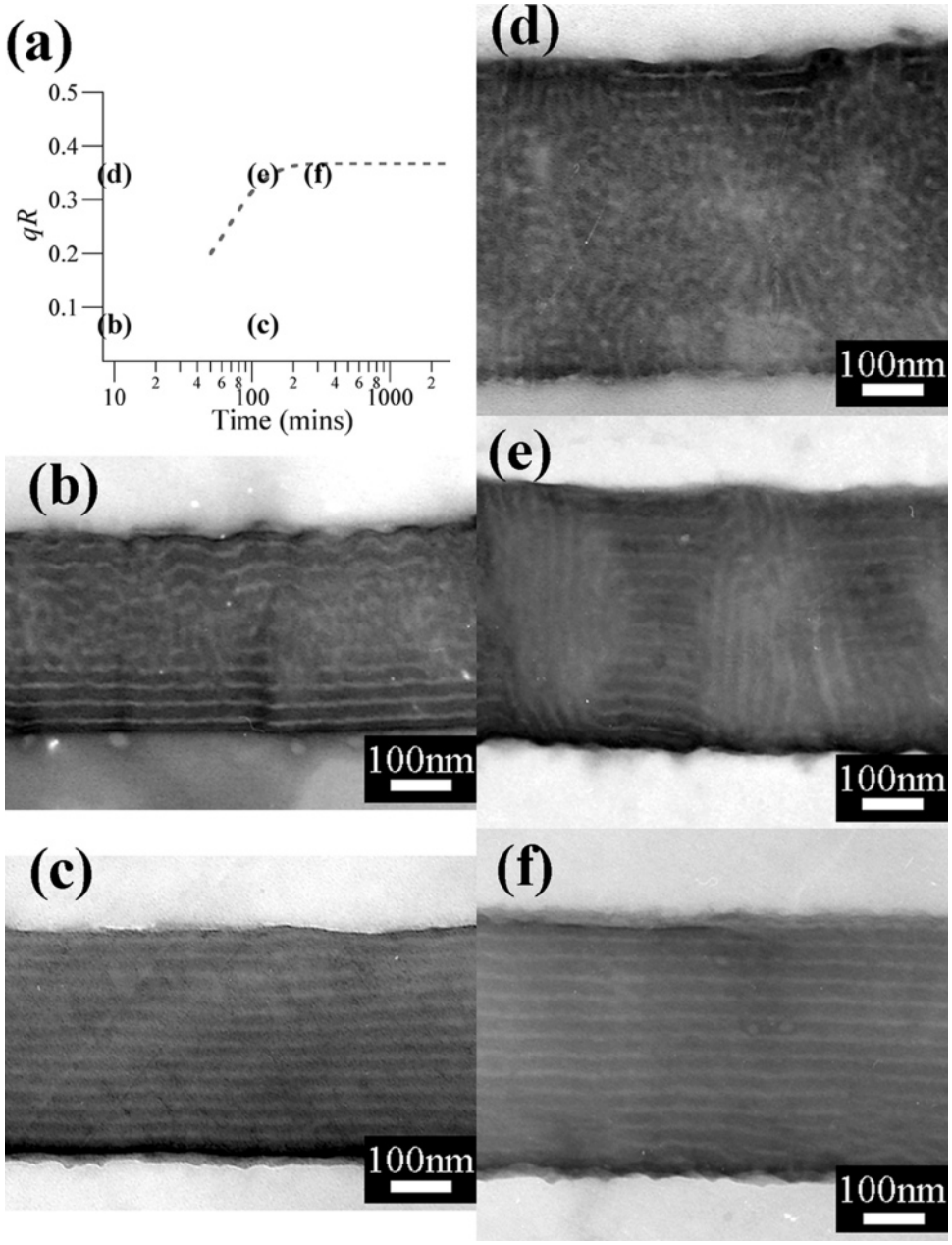

Figure 11. Cross-sectional TEM of 38K−36.8K PS-*b*-PMMA on S_ITO (b, c) and UC_ITO (d−f) substrates as a function of annealing time at 200 °C. Each of (b)−(f) is summarized in (a) in terms of their annealing time and ITO substrate roughness. Also shown in this figure is the locus of the crossover behavior as extracted from Figure 8 for 38K−36.8K PS-*b*-PMMA.

Guided by the AFM results for PS-*b*-PMMA(38K−36.8K) in Figure 8, we identified key annealing times at 200 °C that are above and below the time, $t_{qR=0.32}$ (∼100 min), when the PS-*b*-PMMA surface began to show signs of terracing on the polyimide substrate. These select annealing times are shown in Figure 11a along with the locus of the transition time as a function of q_sR extracted from Figure 8. Each of the symbols (b−f) in Figure 11a denotes the annealing time and the roughness of ITO substrate used in preparing thin films whose cross-sectional TEM images are shown in Figure 11b−f, respectively.

After 10 min of annealing, the PS-*b*-PMMA film on S_ITO already has a significant parallel lamellar portion closest to the substrate side (Figure 11b). A fully parallel thin film is observed on this substrate after 120 min (Figure 11c) of annealing, though this state was possibly reached at an earlier time. By contrast, after 10 min of annealing on the UC_ITO, the film has no dominating structure (Figure 11d) with both parallel and nonparallel domains present. After 120 min (Figure 11e) the film has become well ordered, but a significant portion of the cross section is still in a nonparallel orientation. After further annealing (to 300 min) a fully parallel state was attained (Figure 11f). Thus, these TEM images corroborate the previous observations that substrate roughness significantly slows parallel lamella formation.

There are many phenomena that compete for precedence during the ordering of block copolymer thin films. The initial spun-cast PS-*b*-PMMA thin films will exist in a nonequilibrium disordered state. Annealing results in a fast "quench" into the ordered regime of the block copolymer phase diagram. Because of the role of fluctuations and in the absence of an external field, this phase transition is thought to be first order and hence characterized by nucleation and growth dynamics.[39] An external field, for example a bounding surface with a preferential attraction to one component of the block

copolymer, can effectively increasing the magnitude of the "quench" with the result of enhanced and possibly second-order, surface directed microphase separation. Moreover, one would expect the size of the region of influence of surface directed ordering to be directly related to the strength of the preferential interaction at the surface, i.e., δ_{subs} or δ_{air} with the block copolymer components.

Hence, ordering in substrate-supported thin block copolymer films is a competition between bulk ordering and the directed ordering from the substrate and air surfaces. For example, a thin block copolymer film bounded by two neutral surfaces is bereft of the surface directed ordering; ordering might be expected to occur at the slower "bulk" rates. A perpendicular orientation is observed in such cases because there is less entropic confinement to long-range order within the in-plane directions of the thin film.

In our experimental system, we argue that the air surface is neutral; thus, the substrate surface provides the only external field. Increasing the substrate roughness diminishes the strength and hence the region of influence of the substrate surface directing field. Above a critical roughness, $(q_sR)_{c,true}$, this field is entirely removed. As the substrate gets smoother below $(q_sR)_{c,true}$, the surface directed ordering of parallel lamellae will dominate over the intrinsic microphase separation kinetics.

This physical phenomenon is quite general, yet there are no reports of substrate roughness-induced perpendicular lamellae in the literature using thin films of other model block copolymer systems. This may be because many of these systems, e.g., poly(styrene)-*block*-poly(isoprene) or poly(styrene)-*block*-poly(2-vinylpyridine), also have strongly nonneutral air surfaces. These upper surfaces will have an equal propensity to direct the growth of parallel lamellae at higher rates than the bulk ordering kinetics, once again leading to a parallel oriented thin film.

4. Conclusions

We have shown that substrate roughness can be used to affect the orientation of block copolymers in thin films. We have found not only that a sufficiently rough substrate can lead to perpendicular orientation of the block copolymer but also that there is a critical substrate roughness, below which the parallel orientation of block copolymers is favored. Moreover, the degree of substrate roughness affects the rate with which this parallel orientation is achieved. Strong evidence to support these conclusions came from TEM, AFM, and dSIMS analysis. However, cross-sectional TEM is an illuminating but demanding technique that cannot easily give quantitative results. The AFM observed critical substrate roughness is understood to be an underestimate of the true critical roughness above which no parallel lamellae can form on the substrate. More extensive depth profiling studies in the future would more accurately determine the true critical roughness.

Given our research, it is unsurprising that previous experiments with rough substrates did not report means to produce perpendicular lamellae. The substrates used by Fasolka et al. were not rough enough.[18] A further experiment which did use significantly rough substrates also used poly(styrene)-*block*-poly(2-vinylpyridine) as the model block copolymer.[40] This system has large differences in the attraction of its component blocks to the air and substrate surfaces. In PS-*b*-PMMA these differences are small and can be overcome with substrate roughness effects. This is a peculiar property of a small set of block copolymers. Hence, one might see a similar development of perpendicular lamellae in thin films with other members of the poly(styrene)-*block*-poly(*n*-alkyl methacrylate) family or the poly(ethylethylene)-*block*-poly(ethylpropylene) system.[41]

Acknowledgment. The authors thank Prof. David Andelman and Drs. Yoav Tsori and Mikihito Takenaka for their insights and assistance. E.S. thanks the Japan Society for the Promotion of Science (JSPS) and the Royal Society for their sponsorship of his research. T.H. thanks JSPS for Grant-in-Aid for Scientific Research under Grant 12305060(A) and a grant from the 21st century COE program, COE, for a United Approach to New Materials Science. E.J.K. acknowledges the support of the US National Science Foundation DMR-Polymers Program under Grant DMR03-07233. The work at UCSB also made use of MRL Central Facilities supported by the NSF MRSEC Program under Award DMR00-80034.

Appendix

Figure 4c indicates that the simple model [$f^{||}_{bulk}(z) =$ constant] does not account for the dSIMS data near the substrate (at $z \sim 0$ nm) and air surface (at $z \sim 250$ nm) interfaces. We considered the possibility that a greater fraction of parallel oriented lamellae formed near these bounding surfaces and modeled such behavior as

$$f^{||}(z) = f^{||}_{bulk} + f^{||}_{subs}e^{-z/z_2^*} + f^{||}_{surf}e^{-(l-z)/z_2^*} \qquad (A)$$

where z_2^* was heuristically set to D. $f^{||}_{subs}$ and $f^{||}_{surf}$ correspond to the excess formation of lamellae at the substrate and surface interfaces. Such a fitting model (with $f^{||}_{bulk} = 0.05$, $f^{||}_{surf} = 0.1$, and $f^{||}_{subs} = 0.17$) was able to account somewhat for the dSIMS data behavior near these surfaces (full line in Figure 4c and its inset). To attain this fit, the thickness of the PMMA substrate wetting layer and the next adjacent PS layer were increased by a factor of 1.65. Additionally, we needed to reduce the size the next full PMMA layer by the same amount. This implies a stretching and a subsequent compression of the parallel lamellae that are adjacent to the rough substrate, though a fuller analysis of this effect is not possible without further experiments.

Examining the dPS-*b*-PMMA (on SC_PIM) film surfaces by AFM images, it was possible to produce AFM micrographs of the type shown in Figure 12, which contained a small fraction of nonperpendicular oriented structures. Height analysis (not shown in the phase image of Figure 12) of a typical defect area suggested a layer of thickness ~10 nm (i.e., the thickness of a PS or PMMA wetting layer) lying on top of the perpendicularly oriented surface, and a magnification of such an area (Figure 12, inset) suggests there is a perpendicular oriented domain running beneath this layer. Although the AFM images qualitatively concur with the dSIMS analysis, i.e., a fraction of the air surface is covered by parallel lamellae, such AFM evidence was rare. It may be that the magnitude of the dSIMS determined surface fraction ($f^{||}_{bulk} + f^{||}_{surf} = 15\%$) is unreliable given the closeness of the wetting layer thickness to the dSIMS resolution limit and the effects of the depth-dependent resolution parameter. As a consequence, although one

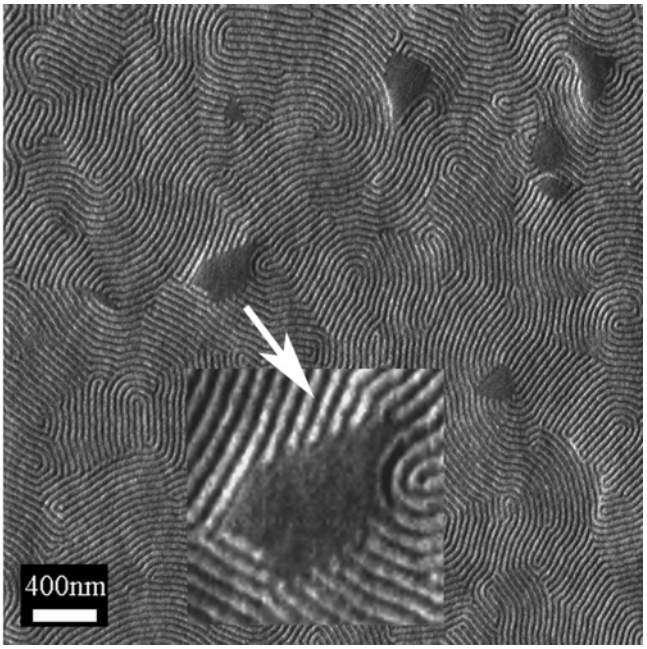

Figure 12. Phase mode AFM images of parallel defects on a mainly perpendicular surface of dPS−PMMA (37K−43K) annealed at 230 °C for 5 h on SC_PIM. Inset shows 0.6 × 0.6 μm magnification.

might expect see some a small fraction of substrate nucleated parallel lamellae, the magnitude of the dSIMS extracted fraction ($f^{\parallel}_{\text{bulk}} + f^{\parallel}_{\text{subs}} = 22\%$) is also subject to the some doubt.

References and Notes

(1) Harrison, C.; Park, M.; Chaikin, P. M.; Register, R. A.; Adamson, D. H. *J. Vac. Sci. Technol. B* **1998**, *16*, 544.
(2) Fredrickson, G. H. *Macromolecules* **1987**, *20*, 2535.
(3) Menelle, A.; Russell, T. P.; Anastasiadis, S. H.; Satija, S. K.; Majkrzak, C. F. *Phys. Rev. Lett.* **1992**, *68*, 67.
(4) Foster, M. D.; Sikka, M.; Singh, N.; Bates, F. S.; Satija, S. K.; Majkrzak, C. F. *J. Chem. Phys.* **1992**, *96*, 8605.
(5) Mansky, P.; Tsui, O. K. C.; Russell, T. P.; Gallot, Y. *Macromolecules* **1999**, *32*, 4832.
(6) Coulon, G.; Ausserre, D.; Russell, T. P. *J. Phys. (Paris)* **1990**, *51*, 777.
(7) Fasolka, M. J.; Mayes, A. M. *Annu. Rev. Mater. Res.* **2001**, *31*, 323.
(8) Mansky, P.; Russell, T. P.; Hawker, C. J.; Pitsikalis, M.; Mays, J. *Macromolecules* **1997**, *30*, 6810.
(9) Rockford, L.; Y, L.; Mansky, P.; Russell, T. P.; M, Y.; Mochrie, S. G. J. *Phys. Rev. Lett.* **1999**, *82*, 2602.
(10) Kim, S. O.; Solak, H. H.; Stoykovich, M. P.; Ferrier, N. J.; de Pablo, J. J.; Nealey, P. F. *Nature (London)* **2003**, *424*, 411.
(11) Kellogg, G. J.; Walton, D. G.; Mayes, A. M.; Lambooy, P.; Russell, T. P.; Gallagher, P. D.; Satija, S. K. *Phys. Rev. Lett.* **1996**, *76*, 2503.
(12) Hashimoto, T.; Bodycomb, J.; Funaki, Y.; Kimishima, K. *Macromolecules* **1999**, *32*, 952.
(13) Amundson, K.; Helfland, E.; Davis, D. D.; Quan, X.; Patel, S. S.; Smith, S. D. *Macromolecules* **1991**, *24*, 6546.
(14) Morkved, T. L.; Lu, M.; Urbas, A. M.; Ehrichs, E. E.; Jaeger, H. M.; Mansky, P.; Russell, T. P. *Science* **1996**, *273*, 931.
(15) Xu, T.; Hawker, C. J.; Russell, T. P. *Macromolecules* **2003**, *36*, 6178.
(16) Fukunaga, K.; Elbs, H.; Magerle, R.; Krausch, G. *Macromolecules* **2000**, *33*, 947.
(17) Kim, S. H.; Misner, M. J.; Xu, T.; Kimura, M.; Russell, T. P. *Adv. Mater.* **2004**, *16*, 226.
(18) Fasolka, M. J.; Harris, D. J.; Mayes, A. M.; Yoon, M.; Mochrie, S. G. J. *Phys. Rev. Lett.* **1997**, *79*, 3018.
(19) Sundrani, D.; Sibener, S. J. *Macromolecules* **2002**, *35*, 8531.
(20) Segalman, R. A.; Yokoyama, H.; Kramer, E. J. *Adv. Mater.* **2001**, *13*, 1152.
(21) Sivaniah, E.; Hayashi, Y.; Iino, M.; Hashimoto, T.; Fukunaga, K. *Macromolecules* **2003**, *36*, 5894.
(22) Sivaniah, E.; Matsubara, S.; Zhao, Y.; Hashimoto, T.; Fukunaga, K.; Mates, T.; Kramer, E. J. *Macromolecules*, in press.
(23) Vitt, E.; Shull, K. R. *Macromolecules* **1995**, *28*, 6349.
(24) Wu, S. In *Polymer Handbook*; Brandrup, J., Immergut, E. H., Eds.; Wiley-Interscience: New York, 1989.
(25) Van Kravelene, D. W. *Properties of Polymers*, 3rd ed.; Elsevier: Amsterdam, 1980.
(26) Yao, S.; Sone, M.; Kamei, E. *Zairyo* **1994**, *43*, 354.
(27) Amundson, K.; Helfland, E.; Patel, S. S.; Quan, X. *Macromolecules* **1992**, *25*, 1935.
(28) Hasegawa, H.; Hashimoto, T. *Macromolecules* **1985**, *18*, 589.
(29) Coulon, G.; Russell, T. P.; Deline, V. R.; Green, P. F. *Macromolecules* **1989**, *22*, 2581.
(30) Yokoyama, H.; Kramer, E. J.; Rafailovich, M. H.; Sokolov, J.; Schwarz, S. A. *Macromolecules* **1998**, *31*, 8826.
(31) Russell, T. P. *Mater. Sci. Rep.* **1990**, *5*, 171.
(32) Fernandez, M. L.; Higgins, J. S.; Penfold, J.; Ward, R. C.; Shackleton, C.; Walsh, D. J. *Polymer* **1988**, *29*, 1923.
(33) Anastasiadis, S. H.; Russell, T. P.; Satija, S. K.; Majkrzak, C. F. *J. Chem. Phys.* **1990**, *92*, 5677.
(34) *D* is found, in increasing order of molecular weight of PS-*b*-PMMA used here, as 28.6, 36.7, 40.2, and 43.5 nm. A full listing is given in ref 22.
(35) Turner, M. S.; Joanny, J. F. *Macromolecules* **1992**, *25*, 6681.
(36) Pickett, G. T.; Witten, T. A.; Nagel, S. R. *Macromolecules* **1993**, *26*, 3194.
(37) Tsori, Y.; Andelman, D. *Macromolecules* **2003**, *36*, 8560.
(38) Carriere, C. J.; Biresaw, G.; Sammler, R. L. *Rheol. Acta* **2000**, *39*, 476.
(39) Hashimoto, T.; Sakamoto, N. *Macromolecules* **1995**, *28*, 4779.
(40) Li, Z.; Qu, S.; Rafailovich, M. H.; Sokolov, J.; Tolan, M.; Turner, M. S.; Wang, J.; Schwarz, S. A.; Lorenz, H.; Kotthaus, J. P. *Macromolecules* **1997**, *30*, 8410.
(41) Ruzette, A.-V. G.; Banerjee, P.; Mayes, A. M.; Pollard, M.; Russell, T. P.; Jerome, R.; T, S.; Hjelm, R.; Thiyagurajan, P. *Macromolecules* **1998**, *31*, 8509.
(42) Mullins, W. W. *Acta Metall.* **1958**, *6*, 414. See also: Gangulee, A. *J. Appl. Phys.* **1974**, *45*, 3749.

MA0482157